Materials Transactions, Vol. 45, No. 7 (2004) pp. 2073 to 2077
Special Issue on Grain Boundaries, Interfaces, Defects and Localized Quantum Structures in Ceramics

Effect of $MgAl_2O_4$ Spinel Dispersion on High-Strain-Rate Superplasticity in Tetragonal ZrO_2 Polycrystal

Koji Morita*, Keijiro Hiraga, Byung-Nam Kim and Yoshio Sakka

National Institute for Materials Science, Tsukuba 305-0047, Japan

The effect of second phase dispersion on high-strain-rate superplasticity was examined in tetragonal ZrO_2 dispersed with 30 vol% $MgAl_2O_4$ spinel. The spinel particle enhances the diffusivity of ZrO_2 by supplying small amounts of aluminum and magnesium into ZrO_2 and suppresses grain growth by grain boundary pinning. After superplastic flow, the spinel particles highly elongate along the tensile direction. In the spinel particles, intragranular dislocations were observed, indicating that the spinel particles may contribute to the relaxation of stress concentrations around grain junctions exerted by grain boundary sliding. Comparison with earlier studies suggests that the dispersion of spinel particles can attain high-strain-rate superplasticity in tetragonal ZrO_2 through providing the following positive factors simultaneously; (i) the suppressed grain growth, enhanced accommodation process due to the accelerated (ii) diffusivity and (iii) stress relaxation.

(Received January 29, 2004; Accepted March 15, 2004)

Keywords: *tetragonal zirconia polycrystal, high-strain-rate superplasticity, accommodation process, intragranular dislocation*

1. Introduction

Since Wakai *et al.*[1] has firstly reported superplastic flow of tensile elongation of $e_f \approx 170\%$ in a fine-grained tetragonal ZrO_2 polycrystal, superplasticity has been attained in several fine-grained ceramics.[2–11] In the most ceramics, however, available strain rates for attaining superplastic flow are limited to 10^{-3}–$10^{-5}\,s^{-1}$.

Recently, we attained high-strain-rate superplasticity (HSRS) in particle dispersed ceramic composites; Al_2O_3-spinel-ZrO_2[12] and ZrO_2-spinel.[13] For a 30 vol% $MgAl_2O_4$ spinel dispersed tetragonal ZrO_2 polycrystal,[13,14] the e_f-value exceeds ≈250% at 1823 K and at an initial strain rate of $\dot{\varepsilon}_0 \approx 0.7\,s^{-1}$. Although the grain size of the ZrO_2-spinel composite is almost similar to that of monolithic ZrO_2,[4,5,8] the spinel dispersion heightens the available strain rate by about 10^3 times for attaining a similar tensile ductility in monolithic ZrO_2.

In earlier studies, the effect of second phase dispersion on superplastic flow has also been examined in several ZrO_2 based composites, in which Al_2O_3[5,15] and mullite ($3Al_2O_3 \cdot 2SiO_2$)[7] particles were dispersed to obtain fine-grained microstructure at high-temperatures. In particular, the flow behavior of Al_2O_3 dispersed tetragonal ZrO_2 was examined for various amounts of Al_2O_3 ranging from 20 to 80 mass%.[11] However, these composites did not exhibit HSRS as in the present ZrO_2-spinel composite. This suggests that the spinel particles play an important role in the attainment of HSRS in tetragonal ZrO_2.

The present study was therefore performed to examine the effect of spinel particle dispersion on HSRS in tetragonal ZrO_2 polycrystal.

2. Experimental Procedures

A fine-grained tetragonal ZrO_2 polycrystal dispersed with $MgAl_2O_4$ spinel was prepared by a method described elsewhere.[13] Briefly, 3 mol%-Y_2O_3-stabilized tetragonal ZrO_2 (>99.97%, TZ-3Y, Tosoh Co., Ltd.,) mixed with 30 vol% spinel powders (>99.9%, SP-12, Iwatani Co., Ltd.,) were cold-isostatically pressed at about 400 MPa and sintered at 1673 K for 2 h in air. From the sintered bodies, dog-bone-shaped flat tensile specimens were machined with gauge portions of ${}^t2\text{-}{}^w3\text{-}{}^l10$ or ${}^t2\text{-}{}^w3\text{-}{}^l5$ mm. Constant displacement-rate tensile tests were conducted at 1723–1823 K and at $\dot{\varepsilon}_0 \approx 1.7 \times 10^{-3} - 0.7\,s^{-1}$ under vacuum using an Instron-type tensile machine.

The microstructures of the as-sintered and deformed specimens were examined by transmission electron microscopy (TEM) and scanning electron microscopy (SEM). For TEM observation, thin sheets with a thickness of about 500 μm were cut with a low-speed diamond cutter, mechanically polished to about 100 μm in thickness and further thinned with an Ar ion-milling machine. For SEM observation, the surface of the specimens were mechanically polished and thermally etched at 1573 K for 10 min. The average grain size, d, was determined as 1.56 times of the average intercept lengths of grains.[16] The grain aspect ratio (GAR) was determined from the intercept lengths measured in the directions parallel and perpendicular to the tensile axis.

3. Experimental Results

3.1 As-sintered microstructure

Figure 1 shows a SEM image of the as-sintered ZrO_2-spinel composite. The white and black contrasts correspond to ZrO_2 (Z) and spinel (S) grains, respectively. The spinel particles disperse homogeneously among the ZrO_2 grains. The ZrO_2-spinel composite has equiaxed grains surrounded by sharply faceted boundaries. The initial average grain sizes are ≈0.29 for ZrO_2 and ≈0.42 μm for spinel.

The details of the microstructure were examined using high-resolution TEM and EDS. Figures 2(a) and (b) are typical microstructures of ZrO_2/ZrO_2 and ZrO_2/spinel boundaries, respectively. As shown in the HRTEM images, the lattice fringes of each grain clearly intersect at the boundaries without any second phases. Although TEM observation was performed at more than 10 boundaries, no

*Corresponding author, E-mail: MORITA.Koji@nims.go.jp

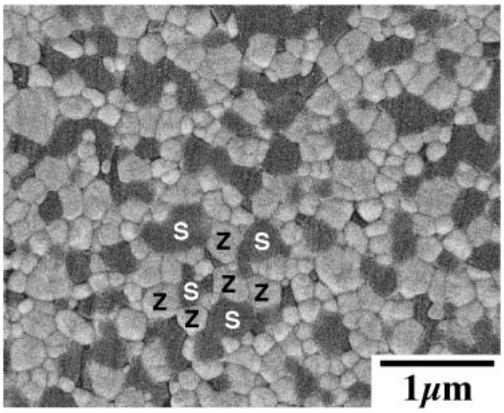

Fig. 1 SEM image of tetragonal ZrO_2 dispersed with 30 vol% $MgAl_2O_4$ spinel.

amorphous phase was found along boundaries and at multiple-grain junctions.

As shown in Fig. 2(c), EDS spectra taken from ZrO_2 grain interiors show a trace of aluminum and magnesium. For ZrO_2/ZrO_2 boundaries, although the intensity of magnesium is almost the same as that of grain interiors, the amount of yttrium and aluminum is higher in grain boundaries than in grain interiors. This result indicates that, in the as-sintered state, small amounts of aluminum and magnesium dissolve into the ZrO_2 matrix from the dispersed spinel.

The XRD profile of the as-sintered ZrO_2-spinel composite is shown in Fig. 3. For comparison, the XRD profile of monolithic ZrO_2 is also shown. All the peaks can be indexed from tetragonal ZrO_2 and spinel phases. This result suggests that no or little cubic ZrO_2 phase exists in the ZrO_2-spinel composite. After static anneal at 1823 K for 10 min, there was no detectable change in the XRD profile. This means that the tetragonal ZrO_2 and spinel phases are stable at testing temperatures.

3.2 Grain growth behavior

Figure 4 shows static grain growth behavior of ZrO_2 grains as a function of annealing time, t. In order to examine the effect of spinel dispersion and the dissolution of aluminum and magnesium on the grain growth behavior, the data of monolithic ZrO_2 and ZrO_2 co-doped with 0.2 mass%Al_2O_3-0.2 mass%MgO are also shown by closed symbols.

The rate of grain growth is apparently higher in Al_2O_3-MgO co-doped ZrO_2 than in monolithic ZrO_2. Since the grain growth of tetragonal ZrO_2 is governed by lattice diffusion of cations,[17] the data indicate that the dissolution of small amounts of aluminum and magnesium enhances the lattice diffusivity of cations in tetragonal ZrO_2.

For spinel dispersed ZrO_2, the grains grow at almost the same rate as that in monolithic ZrO_2. Second phase dispersion is known to suppress grain growth by the pinning of grain boundaries. On the other hand, the dissolution of aluminum and magnesium from the spinel particles may also enhance the lattice diffusivity of the spinel dispersed ZrO_2 as in the case of Al_2O_3-MgO co-doped ZrO_2. The similar grain growth rate between the monolithic and spinel dispersed ZrO_2 suggests that, for spinel dispersed ZrO_2, the lattice

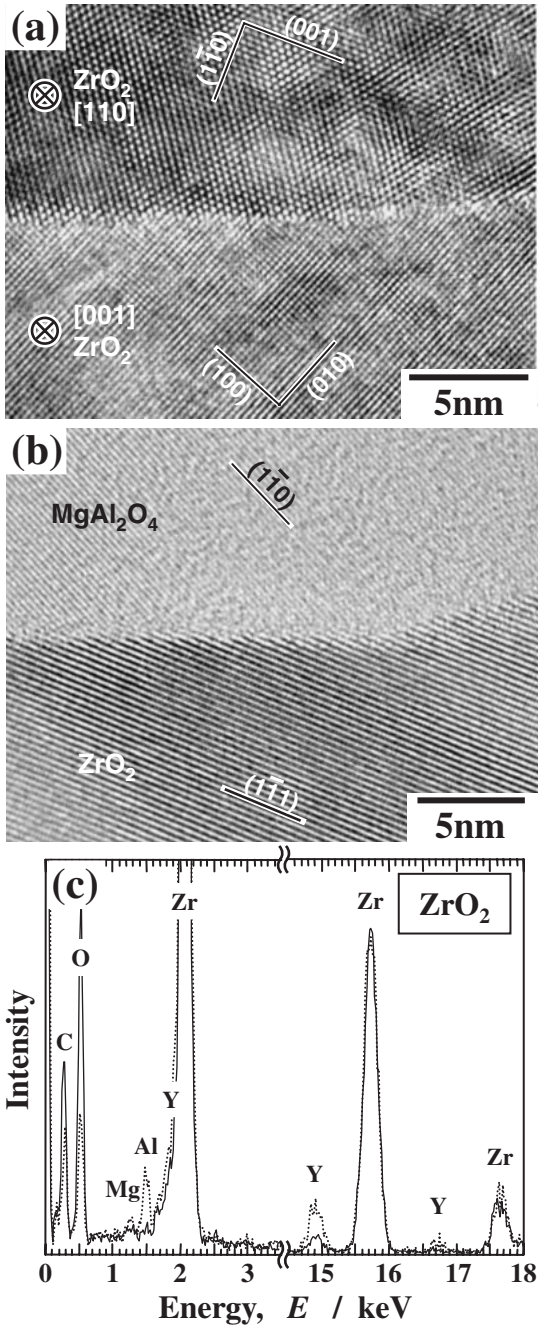

Fig. 2 High-resolution TEM micrographs of (a) ZrO_2/ZrO_2 boundary and (b) ZrO_2/spinel interface, and (c) EDS spectra obtained from the as-sintered ZrO_2-spinel composite.

diffusivity of ZrO_2 would be enhanced by the dissolution of aluminum and magnesium, but the spinel particles would also suppress grain growth of tetragonal ZrO_2 by grain boundary pinning.

3.3 Superplastic flow behavior

Figure 5 shows the superplastic flow behavior of ZrO_2-spinel composite at 1723–1823 K and at $\dot{\varepsilon}_0 \approx 8.3 \times 10^{-2}\,s^{-1}$. The present composite exhibits high-strain-rate superplastic flow of $e_f \geq 200\%$ even at 1723 K and at $\dot{\varepsilon}_0 \approx 8.3 \times 10^{-2}\,s^{-1}$.

The flow behavior is compared with that of monolithic and Al_2O_3 dispersed ZrO_2[4,8,15] in Fig. 6. As compared with

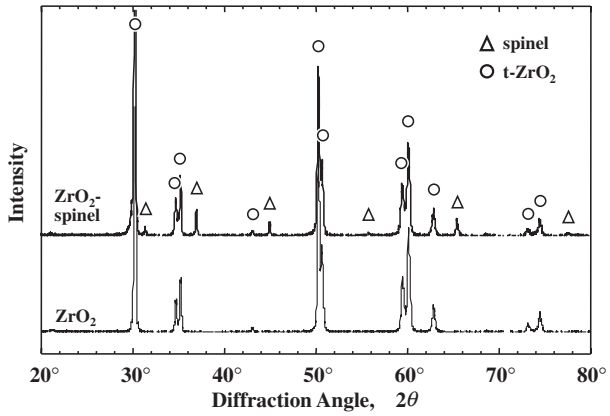

Fig. 3 X-ray diffraction profiles of the as-sintered ZrO_2-spinel composite (top) and monolithic ZrO_2 (bottom). The circles and triangles represent the peaks from tetragonal zirconia (t-ZrO_2) and spinel phases, respectively.

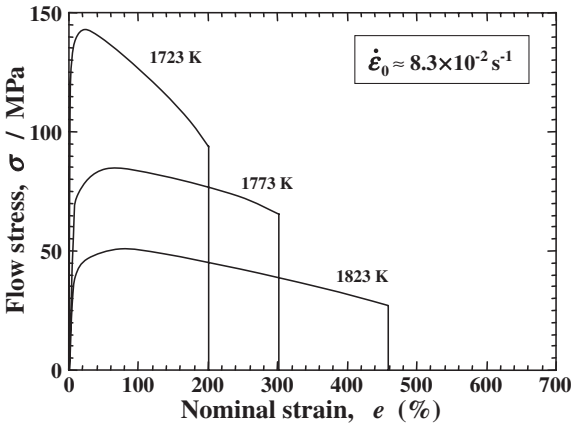

Fig. 5 Temperature dependence of stress-strain curve in ZrO_2-30 vol% spinel composite deformed at $\dot{\varepsilon}_0 \approx 8.3 \times 10^{-2}$ s^{-1} and at 1723–1823 K.

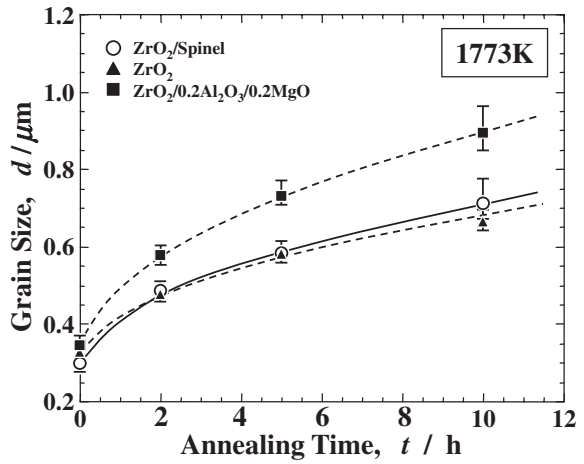

Fig. 4 Static grain growth behavior for 30 vol% spinel dispersed, monolithic and 0.2 mass%Al_2O_3-0.2 mass%MgO co-doped ZrO_2 ceramics at 1773 K.

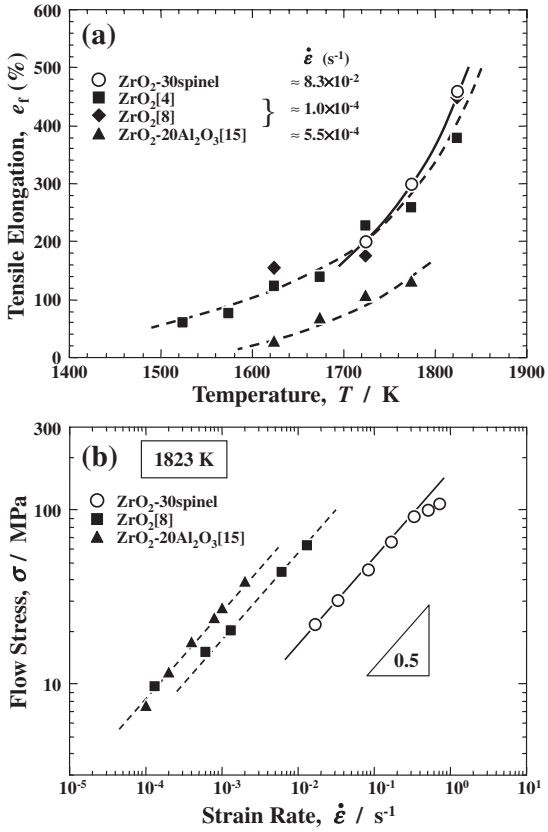

Fig. 6 (a) Temperature dependence of tensile elongation, e_f, at $\dot{\varepsilon}_0 \approx 8.3 \times 10^{-2}$ s^{-1} and (b) flow stress at $\varepsilon = 0.4$, σ, plotted as a function of strain rates, $\dot{\varepsilon}$, at 1823 K. For comparison, earlier data for monolithic ZrO_2[4,8] and ZrO_2-20 vol%Al_2O_3[15] were also shown by closed symbols.

monolithic and Al_2O_3 dispersed ZrO_2, the spinel dispersed ZrO_2 shows almost the same or large tensile elongation at 10^2–10^3 times higher strain rates as shown in Fig. 6(a). With regard to the strain rate sensitivity m estimated from the stress-strain rate relationship in Fig. 6(b), three materials take similar value of $m \approx 0.5$, suggesting that the superplastic flow occurs through the same flow mechanism. Nevertheless, the spinel dispersion can lower the flow stress by 30–40% than that of monolithic and Al_2O_3 dispersed ZrO_2. This indicates that the spinel dispersion improves the superplasticity of tetragonal ZrO_2.

3.4 Microstructure after high-strain-rate superplastic deformation

After high-strain-rate superplastic loading, deformed microstructure was examined by SEM and TEM. Figure 7 shows the SEM micrograph of typical microstructure deformed up to ≈430% at 1773 K and at $\dot{\varepsilon}_0 \approx 8.3 \times 10^{-2}$ s^{-1}. The ZrO_2 grains appear to retain almost the initial equiaxed shape even after large deformation. On the other hand, the spinel particles lie preferentially along the tensile axis. Since the spinel particles also had equiaxed grain shape before deformation (Fig. 1(a)), the elongation must occur during superplastic flow.

A change in GAR during superplastic flow is plotted as a function of local strain, ε_l, in Fig. 8. The GAR-value is apparently different between the ZrO_2 and spinel grains. For the ZrO_2 grains, although GAR increase gradually with ε_l, the value stays less than ≈1.4. For spinel grains, on the other hand, it rapidly increases with ε_l up to ≈1.6.

The deformed substructure of the spinel particles was examined by TEM in Fig. 9. An important feature is

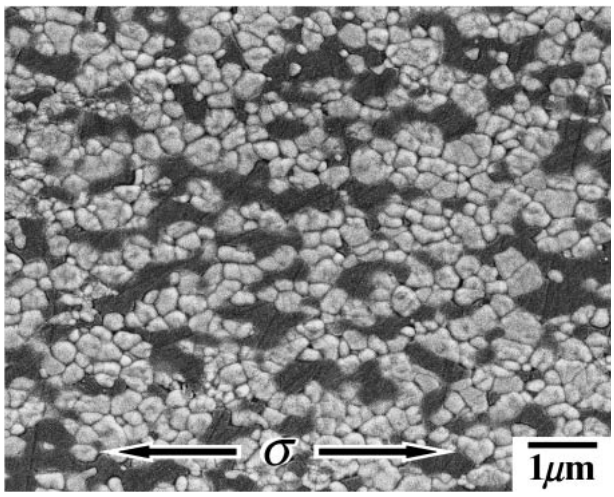

Fig. 7 SEM image of a typical microstructure deformed up to failure of ≈430% at 1773 K and at $\dot{\varepsilon}_0 \approx 8.3 \times 10^{-2}\,s^{-1}$. The tensile axis is horizontal. The deformed microstructure was taken at the vicinity of fracture region.

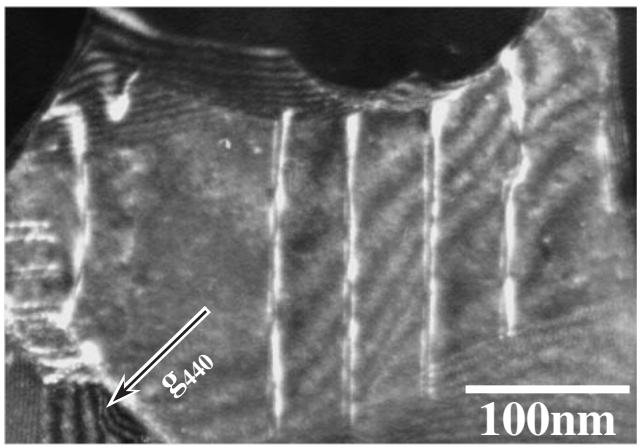

Fig. 9 Dark-field TEM image of spinel grains after deformation up to $\varepsilon \approx 0.2$ at 1773 K and at $\dot{\varepsilon}_0 \approx 0.02\,s^{-1}$. The deformed specimen was cooled rapidly under loading to preserve the microstructures developed during deformation.

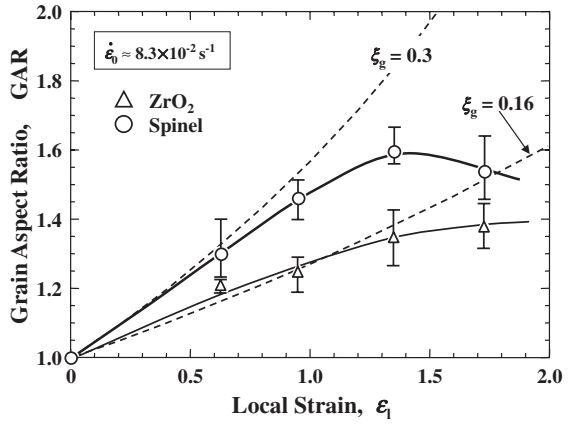

Fig. 8 Grain aspect ratio (GAR) plotted as a function of local strain, ε_l, at 1773 K and at $\dot{\varepsilon}_0 \approx 8.3 \times 10^{-2}\,s^{-1}$. The broken-lines represent the GAR-values expected from the respective contributions of grain strain to total strain at $\xi_g = 0.3$ and 0.16.

noticeably activated intragranular dislocation motion in the particles. Such dislocation motion, including densely aligned dislocations and sub-boundaries, were observed both in the ZrO_2 and in the spinel grains. For the spinel grains, most of the dislocations have a tendency to lie along the elongated direction, suggesting that the dislocation motion may contribute to the grain elongation. Since those dislocation substructures were not observed before deformation, they must be developed during deformation.

4. Discussion

Superplastic deformation has generally been characterized by the m-value defined in the following empirical creep equation

$$\dot{\varepsilon} = A\sigma^{1/m}d^{-p}, \tag{1}$$

where $\dot{\varepsilon}$ is the steady-state strain rate, σ is the true stress, d is the grain size, p is the grain size exponent and A is a constant. For the most ceramics without intergranular amorphous phases, the superplastic flow characterized by $m \approx 0.5$ has been ascribed to grain boundary sliding (GBS).[11,18–20] It is therefore reasonable to explain that the high-strain-rate superplastic flow of the ZrO_2-spinel composite also occurs primarily through GBS.

For deformation by GBS in a polycrystalline matrix, stress concentrations exerted around multiple grain junctions should be accommodated by diffusion processes along boundaries and/or through grains and by plastic deformation. If not, cavity should form around the junctions and this limit the tensile ductility. The present data show that the dispersed spinel particles play an important role in HSRS in tetragonal ZrO_2. The enhanced superplasticity due to spinel dispersion can be ascribed to the following three factors.

The first possible factor is enhanced accommodation process due to the enhancement of cation diffusivity in ZrO_2 grains, because cation diffusion controls the rate of superplastic flow in tetragonal ZrO_2.[19,20] Aluminum and magnesium ions are known to decrease the level of flow stress in ZrO_2.[21,22] The static grain growth behavior and the σ-$\dot{\varepsilon}$ relationship of the present composite suggest that aluminum and magnesium ions dissolve into the ZrO_2 matrix enhance cation diffusivity and thereby result in enhanced accommodation process of GBS.

The second factor is the suppressed concurrent grain growth. The enhanced diffusivity also causes rapid grain growth. The spinel particle dispersion, however, can suppress grain growth by grain boundary pinning as shown in Fig. 4. The fine grain sizes can lower the flow stress as expected from eq. (1). It is apparent from Fig. 6 that the flow stress lowered by the stable fine grain sizes leads to the large elongation at high-strain rates of $\geq 0.1\,s^{-1}$.

Superplasticity of ZrO_2 is not always improved only by the dispersion of particles even if the above two factors work through dispersed particles. According to the earlier study by Suzuki *et al.*,[21] 0.2 wt% Al_2O_3 addition to tetragonal ZrO_2, where the doped Al_2O_3 completely dissolves into ZrO_2 matrix, remarkably decreases the flow stress and attained

HSRS of $e_f \approx 300\%$ at $\dot{\varepsilon}_0 \approx 1.2 \times 10^{-2}\,s^{-1}$ and at 1723 K. They attribute the enhanced superplasticity to the accelerated lattice diffusion of cations due to the Al_2O_3 dissolution. For a further increase in the Al_2O_3 addition, however, the flow stress increases with the precipitation of small Al_2O_3 particles at multiple grain junctions and this results in a decrease in the e_f-value. This suggests that the small Al_2O_3 particles precipitated at multiple grain junctions may retard the predominant GBS process.

For the study of 20 wt% Al_2O_3 dispersed ZrO_2, Owen *et al.*[23] showed that cavities nucleate actively around Al_2O_3 grains. For the ZrO_2-Al_2O_3 composite, the lattice diffusivity of cations must also be accelerated through Al_2O_3 dissolution from the Al_2O_3 grains. Although the bonding strength of ZrO_2/Al_2O_3 boundaries may be lower than that of ZrO_2/ZrO_2 boundaries, the increasing flow stress in the ZrO_2-Al_2O_3 composite shown in Fig. 6(b) suggests that an increase in stress concentrations around the Al_2O_3 grains may enhance cavity nucleation. For tetragonal ZrO_2, rigid second phases such as Al_2O_3 should act as a suppressor for GBS.

Thus, the third factor that leads to HSRS in the present composite is the enhanced accommodation process through the dispersed particles. For the present composite, the spinel particles appear to enhance the relaxation of stress concentrations around multiple grain junctions. A typical microstructural aspect of superplastic ceramics is equiaxed grain shapes retained after large tensile elongation. The present material, however, had highly elongated spinel grains along tensile direction after deformation. This suggests that grain strain of spinel particles, ε_g, contributes to the total strain, ε_{total}.

For ZrO_2 grains, the contribution of ε_g to ε_{total}, ξ_g^Z ($= \varepsilon_g/\varepsilon_{total}$), stays less than 16%, whereas for spinel grains, ξ_g^S reaches $\approx$30%. The ξ_g^S-value tends to increase with an increase in $\dot{\varepsilon}_0$.[14] The difference in the ξ_g-values between the ZrO_2 and spinel grains can be ascribed to a difference in the contribution to the accommodation process. The high ξ_g^S-value suggests that the enhanced accommodation process would significantly take place in the spinel grains rather than in the ZrO_2 grains. Microstructural observation, providing activated dislocations within elongated spinel grains, suggests that the relaxation process caused primary by dislocation motion would be enhanced in the spinel grains in the present composite.

5. Conclusion

The effect of 30 vol% spinel particle dispersion on superplasticity was examined in tetragonal ZrO_2. The spinel particles dispersed into tetragonal ZrO_2 play an important role in attaining HSRS, in which available strain rate was heightened by 10^2–10^3 times in attaining similar tensile ductility in monolithic and Al_2O_3 dispersed ZrO_2. For the ZrO_2-spinel composite, HSRS can be attained by the following three factors. The spinel particles suppress grain growth by grain boundary pinning and thereby lower the flow stress. The spinel particles may enhance the accommodation of the predominant GBS process. The enhanced accommodation arises from the accelerated diffusion due to the dissolution of aluminum and magnesium from the spinel particles and arises from the accelerated stress relaxation of stress concentrations exerted by GBS, through dislocation motion.

Acknowledgements

The authors are grateful to the Mitsubishi Foundation for supporting a part of the present work.

REFERENCES

1) F. Wakai. S. Sakaguchi and Y. Matsuno: Adv. Ceram. Mater. **1** (1986) 259–263.
2) T. G. Nieh, C. M. McNally and J. Wadsworth: Scr. Mater. **23** (1989) 457–460.
3) I. W. Chen and L. A. Xue: J. Am. Ceram. Soc. **73** (1990) 2585–2609.
4) D. J. Schissler, A. H. Chokshi, T. G. Nieh and J. Wadsworth: Acta Mater. **39** (1991) 3227–3236.
5) T. G. Nieh and J. Wadsworth: Acta Mater. **39** (1991) 3037–3045
6) A. H. Chokshi, T. G. Nieh and J. Wadsworth: J. Am. Ceram. Soc. **74** (1991) 869–873.
7) C. K. Yoon and I. W. Chen: J. Am. Ceram. Soc. **73** (1990) 1555–1565.
8) T. Kondo, Y. Takigawa, Y. Ikuhara and T. Sakuma: Mat. Trans., JIM **39** (1998) 1108–1114.
9) K. Nakano, T. S. Suzuki, K. Hiraga and Y. Sakka: Scr. Mater. **38** (1998) 33–38.
10) Y. Takigawa, Y. Yoshizawa and T. Sakuma: Ceramics International **24** (1998) 61–66.
11) T. G. Nieh, J. Wadsworth and O. D. Sherby: *Superplasticity in Metals and Ceramics*, (Cambridge University Press, 1997) pp. 91–119.
12) B.-N. Kim, K. Hiraga, K. Morita and Y. Sakka: Nature **413** (2001) 288–291.
13) K. Morita, K. Hiraga and Y. Sakka: J. Am. Ceram. Soc. **85** (2002) 1900–1902.
14) K. Morita, B. N. Kim, K. Hiraga and Y. Sakka: Mat. Sci. Forum **447-448** (2004) 329–334.
15) F. Wakai and H. Kato: Adv. Ceram. Mater. **3** (1988) 71–76.
16) J. C. Wurst and J. A. Nelson: J. Am. Ceram. Soc. **55** (1972) 109.
17) J. Zhao, Y. Ikuhara and T. Sakuma: J. Am. Ceram. Soc. **81** (1998) 2087–2092.
18) D. M. Owen and A. H. Chokshi: Acta Mater. **46** (1998) 667–79.
19) M. Jiménez-Melendo, A. Domínguez-Rodríguez and A. Bravo-León: J. Am. Ceram. Soc. **81** (1998) 2761–2776.
20) K. Morita and K. Hiraga: Acta Mater. **50** (2002) 1075–1085.
21) T. S. Suzuki, Y. Sakka, K. Morita and K. Hiraga: Scr. Mater. **43** (2000) 705–710.
22) J. Mimurada, M. Nakano, K. Sasaki, Y. Ikuhara and T. Sakuma: J. Am. Ceram. Soc. **84** (2001) 1817–1821.
23) D. M. Owen, A. H. Chokshi and S. T. Nutt: J. Am. Ceram. Soc. **80** (1997) 2433–2436.